Can increased poleward oceanic heat flux explain the warm Cretaceous climate?

Gavin A. Schmidt and Lawrence A. Mysak

Centre for Climate and Global Change Research and Department of Atmospheric and Oceanic Sciences, McGill University, Montréal, Québec

Abstract

The poleward transport of heat in the mid-Cretaceous (100 Ma) is examined using an idealized coupled ocean-atmosphere model. The oceanic component consists of two zonally averaged basins representing the proto-Pacific and proto-Indian oceans and models the dynamics of the meridional thermohaline circulation. The atmospheric component is a simple energy and moisture balance model which includes the diffusive meridional transport of sensible heat and moisture. The ocean model is spun up with a variety of plausible Cretaceous surface temperature and salinity profiles, and a consistent atmosphere is objectively derived based on the resultant sea surface temperature and the surface heat and freshwater fluxes. The coupled model does not exhibit climate drift. Multiple equilibria of the coupled model are found that break the initial symmetry of the ocean circulation; several of these equilibria have one-cell (northern or southern sinking) thermohaline circulation patterns. Two main classes of circulation are found: circulations where the densest water is relatively cool and is formed at the polar latitudes and circulations where the densest water is warm, but quite saline, and the strongest sinking occurs at the tropics. In all cases, significant amounts of warm, saline bottom water are formed in the proto-Indian basin which modify the deepwater characteristics in the larger (proto-Pacific) basin. Temperatures in the deep ocean are warm, 10°–17°C, in agreement with benthic foraminiferal oxygen isotope data. The poleward transport of heat in the modeled Cretaceous oceans is larger than in some comparable models of the present day thermohaline circulation and significantly larger than estimates of similar processes in the present-day ocean. It is consistently larger in the polar sinking cases when compared with that seen in the tropical sinking cases, but this represents an increase of only 10%. The largest increase over present-day model transports is in the atmospheric latent heat transport, where an increased hydrological cycle (especially in the tropical sinking cases) contributes up to an extra 1 PW of poleward heat transport. Better constraints on the oceanic deepwater circulation during this period are necessary before the meridional circulation can be unambiguously described.

Introduction

A common thread that runs through almost all reconstructions of past warm climates such as the mid-Cretaceous, Eocene, and late Pliocene is the presence of a generally reduced pole-to-equator surface temperature gradient [see, for instance, *Huber et al.*, 1995]. Assuming that the solar constant during these periods was roughly the same as at present, this implies that there must have been either major latitudinal changes to the radiation budget or increased poleward heat transport. This poleward transport can be split into three components: (1) the atmospheric sensible heat transport, (2) the atmospheric latent heat transport, and (3) the transport of heat by the oceans. Many previous modeling studies of the mid-Cretaceous (*Barron*, 1983; *Covey and Barron*, 1988; *Crowley*, 1991; *Barron et al.*, 1995,) and the Eocene (*Sloan et al.*, 1995,) have generally concluded that oceanic heat transport must have been greater during these periods. However, the majority of the aforementioned studies have used atmospheric general circulation models (GCMs) in which the sea surface temperature or the poleward oceanic heat flux itself have been prescribed. This implies that the mechanism giving rise to an increased oceanic heat transport and its regional impacts have not been examined in any detail. Hence it is unclear whether a dynamically consistent ocean circulation can exist under the buoyancy and wind forcing derived from these atmospheric GCM experiments.

An increased poleward oceanic heat flux can be ach-ieved in a number of ways: increased transport of heat by the wind-driven upper ocean gyres, increased Ekman transports, or increased transport by the buoyancy-driven thermohaline circulation. The goal of this paper is to determine from a simple coupled atmosphere-ocean model whether heat transported by the thermohaline circulation (THC) can explain all or most of this increase for the warm mid-Cretaceous (100 Ma) period. The THC can transport more heat poleward by three methods: by being more vigorous, by increasing the temperature contrast between the surface and benthic currents, or possibly by a complete rearrangement of the sources of deepwater production.

Some interpretations of deep-sea anoxia and benthic temperature proxy data for the mid-Cretaceous, along with results from simple box models of the deep-sea circulation (*Birchfield*, 1989; *Brass et al.*, 1982,), support the idea that the deep ocean during that period was filled with warm saline bottom water (WSBW). Benthic foraminiferal δ^{18}O data indicate that during this period the middepth waters of the ocean were generally 10°–15°C warmer than today (*Savin*, 1977,). (In today's ocean, temperatures at these middepths (∼1000-1500 m) are generally typical of the abyssal temperatures; however, a possibly much deeper thermocline during the Cretaceous might invalidate such an identification during this period.) WSBW could have been formed at the tropics through evaporation over the extensive shallow seas of the period. However, reconciling this theory with the idea that the oceans transported more heat poleward is difficult. The surface-depth temperature contrast in such an ocean would be rather small, and hence a much greater meridional overturning would be required even to match present-day heat fluxes.

There have been a few purely oceanic modeling studies that use as boundary conditions the surface air temperature and freshwater fluxes derived from previous Cretaceous atmospheric GCM studies. However, these models have not had a high enough vertical resolution to have a reasonable THC [e.g., *Barron and Peterson*, 1990]. Unfortunately, the development of coupled ocean-atmosphere GCMs has not proceeded far enough for reliable paleoclimatic simulations to be carried out. For example, incompatibilities between the components in most of these models mean that they have to contend with the problem of climate drift or the associated problem of flux corrections. Nevertheless, there are a number of simpler ocean models that can be successfully coupled to simple balance models of the atmosphere to give lower-order systems which can be used to study paleoclimates.

The transport of heat by the THC is a crucial mechanism in the climate system, and much work has been done on elucidating the three-dimensional structure of the present-day circulation (*Schmitz*, 1995,). Variability in the heat transport depends mainly upon changes in the oceanic density gradients and possibly upon the surface pathways of the return flow. Changes in the latter are thought mainly to affect the circulation over decadal timescales, and this therefore gives hope that meridional (latitude-depth) models of the THC are able to capture the variability on longer timescales.

The ocean model used in this paper is based on the zonally averaged model of the THC developed by (*Wright and Stocker*, 1991) and extended by (*Wright and Stocker*, 1992) and (*Stocker et al.*, 1992). This ocean model is coupled to a simple energy-moisture

balance model (EMBM) based on that derived recently by (*Fanning and Weaver*, 1996). On its own, the ocean model is able to reproduce the present-day meridional structure of the oceans (*Wright and Stocker*, 1992,) and provide values of the meridional oceanic heat transport which are consistent with current estimates. However, the simplified geometry and crude parameterizations used in the ocean model suggest that it should be regarded more as a conceptual tool rather than as a reconstructive one.

The advantage of the model used here is that it is essentially two-dimensional, and hence many different numerical experiments can be performed in rapid succession. This paper focuses on trying to understand the nature of the oceanic heat transport during the mid-Cretaceous, although the conclusions concerning the production of WSBW will probably also apply to the other warm periods.

The manner in which the experiments are conducted in this paper is slightly nonstandard and is therefore briefly described here. The ocean model is first spun up to a desired "climate" (i.e., the surface temperature and salinity are restored to prescribed profiles). There is considerable latitude in prescribing the initial sea surface temperatures and salinities for a Cretaceous model. The surface temperature is slightly constrained by the data (except at very high latitudes), but there are essentially no serious constraints on the salinity. Because the existence of the thermohaline circulation depends on density contrasts (and hence on both temperature and salinity), this circulation is not constrained by the available surface data.

The ocean-to-atmosphere heat and freshwater fluxes are then diagnosed from the resulting steady state. These fluxes are implicit in the boundary conditions used (given the ocean dynamics). The atmosphere is then constructed by objectively determining various parameters, such as the planetary emissivity and diffusive transports, so that it is in equilibrium with the surface ocean fluxes. Hence further time-stepping of the coupled model produces no climate drift. The coupled model is then perturbed in a number of ways, and various multiple equilibria, typical of such THC models, are found. The poleward heat fluxes in the ocean and in the atmosphere (latent and sensible) can then be calculated. The atmospheric transports are calculated as residuals once the oceanic transport is determined. Since the atmosphere is not dynamic, the values of the computed atmospheric transport act as a further consistency check on the validity of the assumed climate. For instance, an atmospheric heat transport that is an order of magnitude greater than that expected for the period would be inconsistent.

The next section of the paper outlines the basic physics and parameters used in the two components of the model and the procedure that is followed for the numerical experiments. In the third section the experiments are described in some detail, and in the fourth section the results are discussed and compared with estimates and modeling of the THC in the present-day climate. The main conclusions drawn from the study are given in the last section.

Model Description

The governing equations and other technical details of the two model components are described in the appendix. Below, we outline the basic structure, strengths, weaknesses, and validation for each component of the model.

The Ocean Component

The ocean component is derived from the THC model developed by *Wright and Stocker* [1991, 1992] and (*Stocker and Wright*, 1991). The model is derived by zonally averaging the geostrophic momentum equations and the heat and salt advection-diffusion equations across an ocean basin. The equations are closed by parameterizing the east-west pressure gradient in terms of the north-south pressure gradient (in the spirit of (*Stommel*, 1961) and (*Winton and Sarachik*, 1993)). This parameterization is admittedly rather ad hoc but has had some justification in that the simulated THC for the present day is consistent with the observed patterns (*Stocker and Wright*, 1991; *Wright and Stocker*, 1992,).

The ocean basin geometry allowed in this model is necessarily limited, being restricted to choosing a number of interconnected basins in each of which the average width and depth are fixed. Further fine tuning to better represent the geometry and topography is possible by using specific latitude bands for the zonal averaging (*Hovine and Fichefet*, 1994,), but we take the position here that the crudeness of the closure parameterization will not be offset by taking into account small details of the ocean basins. Hence, to model roughly the land-ocean distribution during the mid-Cretaceous, we assume that there is one main ocean basin (the proto-Pacific ocean), which stretches from 80°S to 80°N with a width of 180°, together with an adjacent (proto-Indian ocean) basin (45° width),

which stretches from 40°S to 40°N (Figure 1). The two basins are linked by a strait extending from 40°S to 7.5°S, and the the thermohaline structure at these latitudes is assumed to be the same in each basin. Ocean GCM modeling studies (*Barron and Peterson*, 1989,) suggest that the flow through the Tethys and Arctic Oceans is weak and limited to shallow wind-driven currents. Hence, since this study is concerned primarily with the deep meridional overturning ocean circulation, both of these shallow seas have been excluded. Variations on this geometry have been tried with no qualitative difference in the results.

There are a number of parameters that need to be specified prior to running the model: the horizontal and vertical eddy diffusivities, the constant of proportionality ϵ, used in the closure parameterization, and a parameter that governs how the vertical eddy diffusivity varies with the density gradient. The constant ϵ is defined for a basin that is 60° wide and is always scaled by the width of the basin at each latitude. The values of these parameters have been derived from a combination of open ocean mixing studies, "data" from an ocean GCM, and tuning of the model to the present-day circulation. In particular, the basic vertical diffusivity and closure parameter were chosen to correctly simulate the main thermocline depth and the penetration of North Atlantic Deep Water in a three-basin version of the model for the present-day climate (*Wright and Stocker*, 1992,). Because the closure scheme significantly affects the dynamics of this model, the results of a sensitivity study with respect to this parameter are presented in the next section.

The inclusion of a stability dependent vertical diffusivity [see *Schmidt and Mysak*, 1996] is important so as not to predetermine or limit the amount of mixing that might occur in a possibly less stably stratified Cretaceous ocean. We have also included a representation of the Ekman transport in the ocean model, which initially uses a symmetric profile of the present-day zonal wind stress (*Han and Lee*, 1983,).

The resolution in the horizontal is an average of 10° of latitude, and there are nine variable depth levels in the vertical. The time step in the ocean model is taken to be 14 days.

At the ocean surface, the heat and freshwater fluxes are needed. In the initial spin-up stage, both surface temperature and salinity are restored to a prescribed "climate". This is used solely to prime the ocean component, and hence any variability at this stage is unphysical. At steady state, the fluxes at the surface are calculated and used to construct a consistent atmosphere (see below). In the coupled phase, the fluxes are determined at each time step from the heat and freshwater fluxes produced in the atmospheric model.

Atmospheric Component

The atmospheric model used is a simple zonally averaged energy and moisture balance model that was developed from work by (*Fanning and Weaver*, 1996) and (*Stocker et al.*, 1992). The surface atmospheric temperature and specific humidity are calculated from evolution equations that include the effects of shortwave incoming radiation, longwave outgoing radiation, latent and sensible heat transfers, evaporation, precipitation, and diffusive transport of both heat and freshwater. The atmosphere-to-ocean fluxes can then be calculated and fed into the ocean model. The atmospheric component is time-stepped asynchronously, taking 60 steps for every 1 of the ocean.

The albedo of the planet (*Graves et al.*, 1993,) varies with latitude and is consistent with an ice-free Earth as hypothesized for the mid-Cretaceous (*Clark*, 1988,). Other crucial parameters in this component are the latitudinally dependent diffusivities for both heat and humidity, the planetary emissivity, and the constants that appear in the parameterizations for the precipitation and evaporation. In contrast to some other energy balance models, these parameters are not set a priori but are determined objectively from the oceanic steady state. The derived ocean-to-atmosphere fluxes and the constraint that the atmosphere is in equilibrium with the ocean and space are sufficient for these parameters to be calculated. The process is analogous to the calculation of the frequently used fixed salt-flux condition from the oceanic steady state. In both cases, the solution remains in equilibrium, but the subsequent variability after the system is perturbed is changed to something more realistic. There is one caveat: The determination of these parameters is not guaranteed to give a physically realistic atmosphere. The climate that the model is spun up to must be consistent with the processes used in the atmosphere model. For example, if after an examination of the freshwater and heat fluxes the derived atmospheric transport of moisture or heat is countergradient, there is an inconsistency with a diffusive model for that transport. This puts limits on the range of climates that can be considered, although as will be seen, this is not too onerous a restriction.

One important feature of the coupled model used

here is that the equations can be solved in two distinct ways. Not only can the equations be time-stepped (either to equilibrium or to examine the transients), but the steady state equations can be solved directly (using Newton's method) by employing the procedure developed by (*Schmidt and Mysak*, 1996). This allows us to track the evolution of the steady states, as parameters change, much more efficiently than running each case separately. A useful bonus is that the same calculations can be used to directly examine the linear stability of any state and any possible resonant oscillations around that state.

Model Limitations

Both components of the model are highly simplified and thus leave out many important physical processes. Among these are the atmospheric wind fields and the corresponding wind-driven upper ocean gyres. There is little point in including one and not the other, and to include both would require a coupled ocean-atmosphere GCM (i.e., a three-dimensional model). Hence ignoring them both is at least consistent. One consequence is that the transport of heat by the wind-driven gyres is not included in the energy balance. Hence the residual calculation of the transport of sensible heat by the atmosphere includes this component of the oceanic heat transport as well. However, since the focus of this paper is on whether changes in the deepwater circulation can cause significant changes to the poleward oceanic heat flux, this omission is not crucial, although it needs to be taken into account when discussing the results.

The inclusion of a prognostic moisture transport is an improvement on previous energy balance models, but some aspects of this transport cannot be captured in a diffusive model. For instance, the moisture transport at the tropics is equatorward and counter the gradient of specific humidity. Nonetheless, this formulation has been successfully used previously and is retained for simplicity.

How physically significant is the consistency check when determining the atmospheric parameters, given the shortcomings in the model? Probably, a lack of consistency for particular climates should not be taken too seriously, but since the model is consistent over a large region of the relevant parameter space, the point is moot.

Experiments

The numerical experiments performed represent an attempt to cover the whole range of plausible zonally averaged annual sea surface temperature and salinities for the mid-Cretaceous. To this end, we used smooth meridional profiles for T_0 and S_0 (the initial "climates") in which the polar and equatorial values of temperature and salinity vary. The annual average polar and equatorial temperatures were allowed to vary between $-4°$C and 16°C and between 28°C and 31°C, respectively. Temperatures intermediate to the polar and equatorial values were interpolated using a sine profile. Similarly, the salinity profile used has a double-humped structure with a fixed 0.5-psu (practical salinity unit) dip at the equator, maxima at 30°N and 30°S and minima at the poles. The equatorial salinities were varied between 35 and 36.5 psu, and the polar salinities varied between 30 and 35 psu. Symmetric profiles were used so as not to predetermine whether sinking occurs in the southern or northern hemisphere. From the existence of multiple steady states, the model showed whether it has a preference for asymmetric equilibria or not. Results are presented from only one of these experiments ($T_{eq} = 28°$C, $S_{eq} = 36.5$ psu), since results from the other experiments were qualitatively the same. We also performed an experiment with enhanced radiative forcing (to simulate enhanced atmospheric $p\mathrm{CO}_2$) and sensitivity tests with respect to the strength of the wind stress forcing and closure parameter ϵ used in the ocean model.

Varying the Surface Profiles

The equatorial values of the initial climate were fixed as described above, and the polar temperature and salinity (T_p, S_p) varied for each model run. The shaded region in Figure 2 shows the range of polar salinities and temperatures over which the coupling procedure produced a consistent and physically reasonable atmosphere. The dot-dashed line cutting across the figure is an indication of the relative density of the polar and tropical surface waters at the oceanic steady state. States below the line favor the creation of warm saline bottom water, while states above the line produce their most dense waters at the poles. The degree of shading in each box is a measure of the maximum strength of the total oceanic heat transport for the given (T_p, S_p) pair over all the steady states found. It is clear that the cooler the polar waters in the initial climate, the higher the total heat transport.

The highest values of that transport occur with the saltiest and coolest poles. However, the difference between cases with tropical sinking and those with polar sinking is minimal. The cases with the least efficient heat transport lie roughly in the transition zone.

To illustrate the results of the experiments, only two cases will be highlighted: Case A, with $(T_p, S_p) =$ (5°C, 34.75 psu), is illustrative of those cases with polar sinking, and case B, $(T_p, S_p) =$ (5°C, 30 psu), is representative of the cases with WSBW. The choice of $T_p = 5$°C is made, since it produces a temperature profile that is most typical of the data. Cases with the same initial temperature profile are taken so that (roughly) the amount of total poleward heat transport is the same. The steady states (equilibria) reached after the initial spin-up procedure are basically symmetric in both cases and, as expected, are unstable to finite disturbances.

We found a number of other equilibria for each case (see Table 1), some of which are linearly stable. Figures 3 and 4 show the temperature, salinity, meridional stream function, atmospheric temperature, and specific humidity of the stable equilibria. The first (Figure 3a) is characterized by strong sinking near the northern boundary in the proto-Pacific basin and by weak sinking at the southern tropics in the smaller proto-Indian basin. The temperature of the deep water (about 10°C) is hence an average of the tropical and polar surface temperatures and is consistent with the paleoclimatic data. The atmospheric temperature profile indicates that it is 4°C warmer in the north than in the south due to the asymmetry of the oceanic heat transport. The other stable steady state for this case (Figure 3b) is characterized by sinking in the southern midlatitudes and quite vigorous sinking at the southern boundary of the smaller basin. The deep water temperature in this case is a warm 15°C, with the surface temperature above the southern ocean around 2°C warmer than the north.

Figures 4a and 4b show the stable states for case B. They are characterized by strong sinking in both basins between 30°and 40°S (Figure 4a) or between 30°and 40°N (Figure 4b) and by considerably warmer deepwater temperatures (over 17°C) than in case A. The poleward oceanic heat transports in this case are a smaller fraction of the total poleward transport than found in case A (Figures 5 and 6). Hence the surface temperature difference between the poles is only around 2°C.

All the stable transport patterns shown in Figures 3 and 4 have shallow surface features at the tropics which are typical of the wind-driven component of the meridional circulation. Also, all examples show the bowing up of the isotherms and lines of constant salinity at the equator. The overturning strength of the deep circulation in the larger basin is around 30 Sv (sverdrup). In the smaller basin, there is slightly more variability between the states, with the strength ranging from 3 to 7 Sv.

It is also interesting to examine the heat transports in the model. Since the cases chosen for illustration have similar polar temperatures, the total amount of polar heat transport necessary to maintain the climate is roughly the same, around 7 PW (1 PW = 10^{15} W). There are, however, differences in the amount of heat transported by the oceans (Figures 5 and 6). The steady states for case A (Figures 5a and 5b) have the greatest oceanic heat transport (significantly, in the case of Figure 5a). There are also quite large differences in the atmospheric latent heat transport. In case B, there is a significantly stronger hydrological cycle, and hence larger latent heat transports, as shown in Figures 6a and 6b.

Increased Radiative Forcing

There is some evidence that the atmospheric CO_2 concentration during the Cretaceous was between 5 and 10 times higher than the current value (*Berner*, 1990,). This is very likely to have been a contributing factor to the high temperatures inferred from the proxy data. In most simple energy balance models, increased CO_2 concentration in the atmosphere is simulated by using an increased radiative forcing at the surface that is proportional to the natural logarithm of the concentration (*Mitchell*, 1989,). This corresponds to an extra 10 W m^{-2} for $5\times CO_2$. There is some evidence that this increased radiative forcing is slightly stronger at the equator than at the poles (*Ramanathan et al.*, 1987,), but for lack of any reasonable quantification of this effect, we chose to distribute the forcing equally over the latitudes.

Cases A and B described above were redone using this new formulation, but none of the steady states varied significantly from those achieved previously. This can be explained by the way in which the coupling is performed. After spinning up the ocean model with the initial temperature and salinity profiles, parameters in the atmosphere are diagnosed so that it is in steady state with the ocean. The first requirement is that the incoming shortwave radiation be balanced by the outgoing longwave radiation (modeled as $e_P \sigma T_a^4$). If the incoming radiation is increased by

some constant amount, the derived e_P will increase proportionately (in case B, from 0.57 to 0.60). The effect on the atmosphere of this change is felt only in the temperature equation (see equation (A8) in appendix) where both terms appear. They will cancel out almost exactly over land. Over the ocean, there will be increased evaporation (and hence an increased hydrological cycle), as can be seen from (A13) (see appendix). The increase in E and P are such that again the variations in the terms in (A8) affected by the increased radiative forcing cancel out. The minor differences that do arise are caused by small changes in the profile of T_a. There are greater differences in the transient behavior of the model (growth rates of disturbances, etc.), but they remain small. There is also a minor (3–5%) decrease in the atmospheric sensible heat transport.

In a sense, the atmospheric model can be considered to take account of whatever CO_2 level is necessary to maintain the specified initial climate. If it is warm, then the Earth must be behaving more as a gray body (e_P smaller), precisely the behavior one would expect with greater CO_2 levels. The addition of the extra radiative forcing merely readjusts ϵ_P, but, as is clear from the previous paragraph, it changes very little else.

Sensitivity of the Results

The most important unknown parameter in the ocean model is ϵ, the closure parameter for the east-west pressure gradient (see equation (A4)). Reasonable values of the parameter (when results are compared with oceanic GCM output) have ranged from 0.3 to 0.5 [*Wright and Stocker*, 1991, 1992]. Cases A and B were examined as ϵ was smoothly varied through the above range of values. There were no changes of stability or consistency, and only minor changes in the poleward heat transports occurred. Generally, the ocean transports slightly increased with ϵ, as did the latent heat transport. In consequence (since it is calculated as a residual), the sensible heat transport was slightly reduced. There was, however, a minor increase in total heat transport. The percentage changes, however, are of the order of 5–10% over the range of values examined and hence cannot be considered significant.

The zonal wind stress used to force the Ekman transport is a symmetric version of the best estimate of present-day conditions (*Han and Lee*, 1983,). There are geophysical reasons to suppose that the general form of this forcing (i.e., maxima in the trade winds at 15°N and 15°S, maxima of the westerlies at 45°N and 45°S) is likely to have been constant over the long term. However, the strength of the forcing might well have varied greatly. The sensitivity of the results to this strength was tested by varying the strength from 50% to 200% of the present-day values. The component of the oceanic heat flux carried by the Ekman transport would be expected to vary linearly with the amplitude of the wind, and so variation with this parameter allows us to determine the relative importance of the Ekman transport and the thermohaline circulation.

For cases A and B, there is indeed a linear dependence of the maximum poleward oceanic heat flux on the strength of the wind stress. There is, generally, between a 0.4-PW and 0.6-PW increase in the flux as the wind is increased from 50% to 100%. This implies that at midlatitudes the Ekman transport supplies about half of the poleward transport of heat. For further increases in the wind stress, the linear dependence remained, but for increases greater than 130%, the objectively determined atmosphere became inconsistent. There were no changes in stability for any of the steady states in the examined range.

Discussion

There are likely to be many contributing causes to the high global average temperatures seen during the mid-Cretaceous. Albedo changes due to a lack of permanent ice sheets, and the change in land-sea distribution combined with an elevated concentration of atmospheric CO_2, will have caused a general warming. Nonetheless, atmospheric GCM experiments have not been able to simulate fully either the degree of warming or the reduced equator-to-pole thermal gradient without making an assumption of increased heat transport by the oceans or by invoking some general change in cloud behavior (*Covey et al.*, 1996,). The possibility of an external cause of the increased temperatures, such as increased solar forcing, should not be forgotten. However, the mechanisms within the climate system that could be responsible for such a warm climate should be investigated thoroughly before they are possibly discounted. What does this study then indicate concerning the role of the oceans?

Compared with the present-day climate (for which the total poleward heat flux has a maximum of about 5 PW), the model indicates that an extra 2 PW (at around 40°N and 40°S) of poleward heat flux is nec-

essary in order to maintain the warm high-latitude temperatures. This heat flux can be broken down into components (atmospheric sensible heat, atmospheric latent heat, and oceanic heat transport) and each discussed separately.

The poleward atmospheric sensible heat transports in all four examples (Figures 5 and 6) have maxima at around 40°N and 40°S of about 3 PW. That is of the same order as the sensible heat transports at present. It should be remembered that these transports are calculated as residuals and therefore contain part of the heat transport that would be carried by the ocean surface gyres not represented in our model. Some atmospheric GCM experiments (*Barron and Washington*, 1982,) have indicated that a reduced equator-to-pole temperature gradient does not necessarily imply a weaker atmospheric circulation. It is possible that the increased latent heat release at the tropics maintains (or even possibly strengthens) the vertically averaged meridional gradient and hence the strength of the winds. This is at least consistent with the use of present-day wind stress forcing in this study. An increase in the monsoonal circulation due to the different continental distribution is also likely. Hence the sensible heat transports in this model are, for the cases shown, reasonable. For some of the cases with extreme polar warming ($T_p > 10$°C, not shown), these transports were far too large to be reasonable, and so these cases are ignored.

The poleward oceanic heat transports show more variability among the cases shown. There is a marked asymmetry between the northward and southward tran-sports in each case due to the asymmetric one-cell circulation seen in Figures 3 and 4. There is a tendency for models in which there is one principal basin, such as this one, to prefer asymmetric circulations. The instability associated with symmetric circulations has been explained by (*Schmidt and Mysak*, 1996), among others. Usually, there are at least two stable states with opposing circulations (such as in cases A and B), and under stochastic forcing from the atmosphere it is usual that flips between the steady states generally occur on millennial timescales. Hence no asymmetry would necessarily be seen in the low-resolution proxy records available. The oceanic meridional component of the poleward flux in each case has a maximum of around 2 PW in the sinking hemisphere and a smaller local maximum of around 0.6 PW in the other hemisphere. The fluxes are consistently greater in the polar sinking cases than in the tropical sinking ones, due mainly to the slightly cooler bottom waters, but this difference amounts to only 10–15%.

Some features of the modeled ocean circulation are worth pointing out. Chief among these is the role of the proto-Indian ocean in the production of WSBW in all cases. Unlike the geography of the modern world, the proto-Indian ocean is not directly connected to a significant source of deep water. Today, the mixing of Antarctic bottom water and North Atlantic Deep Water that occurs in the Antarctic Circumpolar Current gives rise to the common water that fills both the Indian and Pacific Oceans. Conversely, during the Cretaceous, if there were polar sources of deep water, these will have been localized, and in the absence of any circumpolar current, they will not have filled the proto-Indian basin so readily. This allows sinking of water in the basin even though it is not as dense as the polar source waters. This modifies the average temperature of the waters in the proto-Pacific so that they are noticeably warmer than sea surface temperatures in the main sinking region.

Present-day modeling of the meridional circulation has produced maximum poleward heat transports of around 1.6 PW in a coupled three-basin zonally averaged model (*Stocker et al.*, 1992,) and 2.0 PW in an ocean-only version (*Wright and Stocker*, 1992,). Values of key parameters in the coupled model were slightly different from those used here, specifically, $K_v = 1 \times 10^{-4}$ m^2 s^{-1} and $\epsilon = 0.5$. These changes have the effect of increasing the overturning stream function by around 20% over that seen here. Hence the values found in the Cretaceous cases seem to be significantly larger (by about 0.5 PW). Compared with the ocean-only model, the increases appear less significant.

Estimates of the current total poleward oceanic heat flux vary from a maximum of 3 PW (at 30°N and 30°S) (*Carissimo et al.*, 1985,) to a more accepted 2 PW in more recent satellite studies (*Trenberth and Solomon*, 1994,) and in direct observations (*Bryden and Hall*, 1980,). Of that, half is normally attributed to the surface gyres. The transports in this study are significantly above these estimates, although this may be due to a systematic bias in the model.

There are, however, large increases in the atmospheric latent heat transports as compared with present-day estimates or models, and these account for the majority of the extra poleward transport necessary to maintain the warm high latitudes. This is clearly more evident in the tropical sinking case. This is not surprising, given that a more vigorous hydrolog-

ical cycle is necessary in order to maintain the strong salinity gradients that drive the reversed circulation. Maxima of 2.5–3.4 PW in the latent heat transport are found, instead of the 1.3 PW (*Sellers*, 1965,) that is estimated today or the 2.4 PW in similar present-day models (*Stocker et al.*, 1992,). Similar results were also seen in coupled GCM simulations of CO_2 -induced warmer climates in the work by (*Manabe and Bryan*, 1985).

What further data could help refine these conclusions and restrict the range of possible circulations? Better data on anoxia in the open ocean, or near the poles, could indicate if large amounts of polar sinking were taking place. Also, more benthic temperature data could help determine whether two or more significantly different deepwater masses were present in the proto-Pacific. Estimates of changes in surface gyre transports from OGCM models will also help narrow the possibilities.

Conclusions

The oceanic circulations presented here seem to be consistent with atmospheric GCM results and with what little data there are. The poleward transport of heat by the thermohaline circulation does increase over that seen in models of the present-day circulation. Transports are also significantly larger than present-day estimates of the meridional cell transports. This increase, combined with a much more vigorous hydrological cycle, may provide enough heat transport to sustain the warm high-latitude climate. The results also indicate that because of the unusual geography and the increased hydrological cycle, some amounts of WSBW may have been ubiquitous, but that does not rule out an additional polar source of deep water.

While further research into atmospheric or solar effects is clearly desirable, the results of this study seem to indicate that it is not necessary to postulate, for instance, a completely different cloud regime during the Cretaceous in order to explain the warm climate. Unfortunately, given the paucity of data, the results so far do not allow an unambiguous description of the oceanic meridional circulation.

Appendix: Model Details

The complete details and justification of the oceanic model, the atmospheric model, and the methods of solution can be found in the original references [*Wright and Stocker*, 1991, 1992; *Fanning and Weaver*, 1996; *Schmidt and Mysak*, 1996]. The details that are included here are those that are relevant to the discussions in the text.

The basic equations solved for in the ocean model arise from the zonal averaging of the governing momentum and tracer equations in spherical coordinates. Time dependence arises in the two advection-diffusion equations for the potential temperature (T_{oc}) and salinity (S). Continuity implies the existence of a stream function (ψ) which can be solved for directly by parameterizing the east-west pressure gradient ($\Delta p/\Delta\Lambda$) and by making the hydrostatic and Boussinesq approximations. The equation of state is fully nonlinear and pressure dependent. The equations to be solved are thus as follows:

$$\frac{\partial T_{oc}}{\partial t} + J(\psi, T_{oc}) = \nabla \cdot \left(K_h \frac{\partial T_{oc}}{\partial s}, K_v \frac{\partial T_{oc}}{\partial z} \right) \quad \text{(A1)}$$

$$\frac{\partial S}{\partial t} + J(\psi, S) = \nabla \cdot \left(K_h \frac{\partial S}{\partial s}, K_v \frac{\partial S}{\partial z} \right), \quad \text{(A2)}$$

$$\frac{2\Omega s R \rho_0}{c} \frac{\partial \psi}{\partial z} = -\frac{1}{Rc} \frac{\Delta p}{\Delta \Lambda} + \frac{\tau}{\delta_M} \mathcal{H}(z + \delta_M), \quad \text{(A3)}$$

$$\frac{\Delta p}{\Delta \Lambda} = -\frac{2\pi \epsilon s c^2 g}{3 \Delta \Lambda} \int^z \frac{\partial \rho}{\partial s}\, dz, \quad \text{(A4)}$$

$$\rho = \rho(T_{oc}, S, z), \quad \text{(A5)}$$

where $c = \cos$ (lat); $s = \sin$ (lat); K_h and K_v are the horizontal and (stability dependent) vertical diffusivities, respectively; ρ_0 is the reference density; R is the radius of the Earth; ϵ is the closure parameter; $\Delta\Lambda$ is the width of the basin; and τ is the zonal wind stress which acts over the mixed layer depth δ_M. The rotation rate of the Earth Ω and the gravitational acceleration g are known constants. We define $\nabla F = (\partial(c^2 F/a^2)/\partial s, \partial F/\partial z)$, $J(f,g) = f_s g_z - f_z g_s$, and $\mathcal{H}$ is the Heaviside function. The boundary conditions at the surface ($z = 0$) are

$$-K_v \frac{\partial T_{oc}}{\partial z} = \begin{cases} \delta_M (T_{oc} - T_0)/\tau_T, & \text{ocean only} \\ -Q_{a-oc}/(\rho_0 C_{\rho w}), & \text{coupled} \end{cases} \quad \text{(A6)}$$

$$-K_v \frac{\partial S}{\partial z} = \begin{cases} \delta_M (S - S_0)/\tau_S, & \text{ocean only} \\ 0.035 F_{a-oc}, & \text{coupled} \end{cases} \quad \text{(A7)}$$

where T_0 is the apparent atmospheric temperature (*Haney*, 1971,), S_0 is an approximate surface salinity profile, $C_{\rho w}$ is the heat capacity of sea water, and τ_T and τ_S are the restoring time constants. The values

for the various parameters are shown in Table A1. The heat and freshwater atmosphere-to-ocean fluxes, Q_{a-oc} and F_{a-oc}, are defined in (A13) and (A14).

The atmospheric model takes the form of two zonally averaged prognostic equations, one for the surface air temperature and one for the surface specific humidity, each of which varies with latitude and time:

$$\begin{aligned} C_{\rho a} H_a \rho_{\rm air} \frac{\partial T_a}{\partial t} &= (1-a)(1-\alpha_P) Q_{SW} + Q_{SH} \\ &\quad -\epsilon_P \sigma T_a^4 - \epsilon_A \sigma T_a^4 \\ &\quad +\epsilon_O \sigma T_{oc}^4|_{z=0} + x_L P \\ &\quad +\frac{C_{\rho a} H_a \rho_{\rm air}}{R^2} \frac{\partial}{\partial s}\left(c^2 K_T \frac{\partial T_a}{\partial s} \right), \end{aligned} \tag{A8}$$

$$\begin{aligned} H_q \rho_{\rm air} \frac{\partial q}{\partial t} &= \frac{H_q \rho_{\rm air}}{R^2} \frac{\partial}{\partial s}\left(c^2 K_q \frac{\partial q}{\partial s} \right) \\ &\quad +(E-P), \end{aligned} \tag{A9}$$

where $C_{\rho a}$ is the specific heat capacity of air; H_a and H_q are scale heights; x_L is the latent heat of evaporation of water; ϵ_P, ϵ_A, and ϵ_O are the planetary, atmospheric and oceanic emissivities, respectively; σ is the Stefan-Boltzmann constant; K_T and K_q are the meridional diffusive transport coefficients for heat and freshwater; α_P is the planetary albedo; Q_{SW} is the incoming shortwave radiation; and a is the fraction of that radiation absorbed by the ocean. The evaporation (E), precipitation (P), and sensible heat flux (Q_{SH}) are determined from the surface sea and air temperatures ($T_{oc}(y, z=0), T_a$), the relative humidity, and the saturation specific humidity of the atmosphere:

$$P = \max\left[0, P_0(q - 0.85 q_{\rm sat}(T_a))\right], \tag{A10}$$

$$E = \max\left(0, E_0(q_{\rm sat}(T_{oc}|_{z=0}) - q)\right), \tag{A11}$$

$$Q_{SH} = Q_0(T_{oc}|_{z=0} - T_a). \tag{A12}$$

The scale factors and distribution of zonally averaged precipitation among the basins are subsumed in the bulk transfer coefficient P_0. E_0 is a modified spatially varying Dalton number, and since the surface winds are not explicitly calculated, the sensible heat transfer coefficient, Q_0, is taken to be a constant. The heat and freshwater fluxes into the ocean are then calculated as follows:

$$\begin{aligned} Q_{a-oc} &= aQ_{SW} - Q_{SH} + \epsilon_A \sigma T_a^4 \\ &\quad -\epsilon_O \sigma T_{oc}^4|_{z=0} - x_L E, \end{aligned} \tag{A13}$$

$$F_{a-oc} = P - E. \tag{A14}$$

The atmosphere-to-surface fluxes only occur over the oceans since the land is considered inactive. Hence it is also necessary to specify how the (zonally averaged) precipitation is distributed among the ocean basins.

At coupling, the heat and freshwater fluxes are derived from the ocean model. The sea surface temperature is likewise set, and the atmospheric temperature is determined from the apparent atmospheric temperature used in the Haney restoring term. Assuming a steady state of the atmosphere, this determines (in order) (1) the planetary emissivity (from the balance at the top of the atmosphere); (2) the evaporation at any point (from equation (A13)); (3) the precipitation at any point (from equation (A14)); (4) the zonally averaged precipitation (and hence the distribution of precipitation among the basins, P_0); (5) the relative humidity and the Dalton number E_0 (from equation (A11)); (6) the meridional gradients of q and T_a; and finally (7) the diffusive constants K_T and K_q as derived from the integrated versions of (A8) and (A9).

There are a number of points where this procedure may break down. At step 2 or 3, the evaporation or precipitation calculated may be negative; at step 5, E_0 may be negative; and in the final step, the diffusive constants may be negative. If any of these situations arise, there is a contradiction between the climate as initially specified in the ocean surface boundary conditions and the processes that are modeled in the atmosphere. However, although this can occur, there are large regions of parameter space where it does not (Figure 2). Some criticism may be made of the fact that parameters crucial to the atmosphere are determined from an admittedly imperfect ocean model. We argue that since no reliable data are available for paleoclimatic validation of these parameters, it is better to construct a consistent atmosphere that is a slave to the ocean. In that way, the transports in the atmosphere are calculated as a residual, given the transports in the ocean. The coupled model is then at equilibrium (no climate drift), and any errors are effectively due to those in the ocean model alone.

The equations can either be solved by time-stepping the equations asynchronously or by solving directly for the steady state. The latter approach involves linearizing the discretized equations around any particular state and then using Newton's method to iterate to the steady state. Convergence of this method is not guaranteed, but when it occurs, the method is much more efficient than time stepping.

Acknowledgments. We are grateful for the help of

Halldor Björnsson with the coding of the model and to Martin Hoffert, Ken Miller, Mark Leckie, and an anonymous reviewer who constructively criticized an earlier version of the paper. This work was funded by NSERC and AES grants awarded to L.A.M.

*

References

Barron, E. J. 1983: A warm equable Cretaceous: the nature of the problem: *Earth Sci. Rev.*, *19*, 305–338, .

Barron, E. J., P. J. Fawcett, W. H. Peterson, D. Pollard, and S. L. Thompson 1995: A "simulation" of mid-Cretaceous climate: *Paleoceanography*, *10*, 953–962, .

Barron, E. J., and W. H. Peterson 1989: Model simulation of the Cretaceous ocean circulation: *Science*, *244*, 684–686, .

Barron, E. J., and W. H. Peterson 1990: Mid-Cretaceous ocean circulation: Results from model sensitivity studies: *Paleoceanography*, *5*, 319–337, .

Barron, E. J., and W. M. Washington 1982: Atmospheric circulation during warm geologic periods: is the equator-to-pole surface-temperature gradient the controlling factor?: *Geology*, *10*, 633–636, .

Berner, R. A. 1990: Atmospheric carbon dioxide over Phanerozoic time: *Science*, *249*, 1382–1386, .

Birchfield, G. E. 1989: A coupled ocean-atmosphere model: temperature versus salinity effects on the thermohaline circulation: *Climate Dynamics*, *4*, 57–71, .

Brass, G. W., J. R. Southam, and W. H. Peterson 1982: Warm saline bottom water in the ancient ocean: *Nature*, *296*, 620–623, .

Bryden, H., and M. M. Hall 1980: Heat transports by currents across 25°N latitude in the Atlantic Ocean: *Science*, *207*, 884–886, .

Carissimo, B. C., A. H. Oort, and T. H. V. Haar 1985: Estimating the meridional energy transports in the atmosphere and oceans: *J. Phys. Ocean.*, *15*, 82–91, .

Clark, D. L. 1988: Early history of the Arctic Ocean: *Paleoceanography*, *3*, 539–550, .

Covey, C., and E. J. Barron 1988: The role of ocean heat transport in climate change: *Earth Sci. Rev.*, *24*, 429–445, .

Covey, C., L. C. Sloan, and M. I. Hoffert 1996: Paleoclimate data constraints on climate sensitivity: the paleocalibration method: *Climatic Change*, *32*, 165–184, .

Crowley, T. J. 1991: Past CO_2 changes and tropical sea surface temperatures: *Paleoceanography*, *6*, 387–394, .

Fanning, A. F., and A. J. Weaver 1996: An Atmospheric Energy-Moisture Balance model: Climatology, interpentadal climate change, and coupling to an OGCM: *J. Geophys. Res.*, page (in press), .

Graves, C. E., W.-H. Lee, and G. R. North 1993: New parameterizations for simple climate models: *J. Geophys. Res.*, *98*, 5025–5036, .

Han, Y.-J., and S.-W. Lee 1983: An analysis of monthly mean wind stress over the global ocean: *Mon. Weather Rev.*, *111*, 1554–1566, .

Haney, R. L. 1971: Surface thermal boundary condition for ocean circulation models: *J. Phys. Oceanogr.*, *1*, 241–248, .

Hovine, S., and T. Fichefet 1994: A zonally-averaged, three-basin ocean general circulation model for climate studies: *Climate Dynamics*, *10*, 313–331, .

Huber, B., D. Hodell, and C. Hamilton 1995: Middle-Late Cretaceous climate of the southern high latitudes: stable isotopic evidence for minimal equator-to-pole thermal gradients: *GSA Bull.*, *107*, 1164–1191, .

Manabe, S., and K. Bryan 1985: CO_2-induced change in a coupled ocean-atmosphere model for climate studies: *J. Geophys. Res.*, *90*, 11,689–11,707, .

Mitchell, J. F. B. 1989: The "Greenhouse" effect and climate change: *Rev. Geophys.*, *27*, 115–139, .

Ramanathan, V., L. Callis, R. Cess, J. Hansen, I. Isaksen, W. Kuhn, A. Lacis, F. Luther, J. Mahlman, R. Reck, and M. Schlesinger 1987: Climate-chemical interactions and effects of changing atmospheric trace gases: *Rev. Geophys.*, *25*, 1441–1482, .

Savin, S. M. 1977: The history of the earth's surface temperature during the past 100 million years: *Ann. Rev. Earth Plan. Sci.*, *5*, 319–355, .

Schmidt, G. A., and L. A. Mysak 1996: The stability of a zonally averaged thermohaline circulation model: *Tellus*, *48A*, 158–178, .

Schmitz, W. J. 1995: On the interbasin-scale thermohaline circulation: *Rev. Geophys.*, *33*, 151–173, .

Sellers, W. D. 1965: *Physical Climatology*: University of Chicago, Chicago: 272pp.

Sloan, L. C., J. C. G. Walker, and T. C. Moore 1995: Possible role of oceanic heat transport in early Eocene climate: *Paleoceanography*, *10*, 347–356, .

Stocker, T. F., and D. G. Wright 1991: A zonally averaged ocean model for the thermohaline circulation. Part II: Interocean circulation in the Pacific-Atlantic basin system: *J. Phys. Oceanogr.*, *21*, 1725–1739, .

Stocker, T. F., D. G. Wright, and L. A. Mysak 1992: A zonally averaged coupled ocean-atmosphere model for paleoclimatic studies: *J. Climate*, *5*, 773–797, .

Stommel, H. 1961: Thermohaline convection with two stable regimes of flow: *Tellus*, *13*, 224–230, .

Trenberth, K. E., and A. Solomon 1994: The global heat balance: heat transports in the atmosphere and ocean: *Climate Dynamics*, *10*, 107–134, .

Winton, M., and E. S. Sarachik 1993: Thermohaline oscillation induced by strong steady salinity forcing of ocean General Circulation Models: *J. Phys. Oceanogr.*, *23*, 1389–1410, .

Wright, D. G., and T. F. Stocker 1991: A zonally averaged ocean model for the thermohaline circulation. Part I: Model development and flow dynamics: *J. Phys. Oceanogr.*, *21*, 1713–1724, .

Wright, D. G., and T. F. Stocker 1992: Sensitivities of a zonally averaged global ocean circulation model: *J. Geophys. Res.*, *97*, 12,707–12,730, .

L. A. Mysak and G. A. Schmidt, Centre for Climate and Global Change Research and Department of Atmospheric and Oceanic Sciences, McGill University, 805 Sherbrooke Street West, Montréal, Québec, H3A 2K6 (e-mail: mysak@zephyr.meteo.mcgill.ca)

March 19, 1996; revised June 4, 1996; accepted June 17, 1996.

This preprint was prepared with AGU's LaTeX macros v4. File paper formatted November 11, 1998.

Table 1. Characteristics of the Steady States (Equilibria) for Cases A and B as Marked in Figure 2

$S_{eq} - S_p$, psu		$T_{eq} - T_p$, °C		Sinking Latitude(s)	Maximum Oceanic Heat Transport, PW	Maximum Atmos. Sensible Heat Transport, PW	Bottom Temperature, °C	Stability
South	North	South	North					
				Case A				
1.5	1.5	18.6	18.6	70°N,S & 30°N,S	1.9	3.4	8.6	unstable
6.3	1.2	22.0	18.6	70°N,30°S	2.02	3.2	11.2	unstable
6.3	0.7	22.0	17.6	70°N	2.05	3.2	10.1	stable
4.7	6.5	19.8	21.4	55°S,35°S	2.2	3.7	14.7	stable
				Case B				
5.9	5.9	19.7	19.7	30°N,30°S	1.4	3.7	20.2	unstable
7.3	3.8	20.7	18.6	40°N,60°N	1.7	3.5	14.0	unstable
5.6	7.3	19.1	20.5	40°S	1.9	3.8	17.7	stable
7.1	5.3	20.7	19.3	40°N	1.5	3.5	17.6	stable

Table A1. Constants and Parameters Used in Ocean and Atmosphere Models

Name	Variable	Value
Closure parameter	ϵ	0.45
Vertical eddy diffusivity	K_v	0.44×10^{-4} m^2 s^{-1}
Horizontal eddy diffusivity	K_h	10^3 m^2 s^{-1}
Restoring time constants	τ_T, τ_S	50 days
Mixed layer depth	δ_M	50 m
Reference density	ρ_0	1035 kg m^{-3}
Oceanic time step	Δt_O	14 days
Shortwave incoming radiation	Q_{SW}	$340(1.246 - 0.738 \sin^2(\text{lat}))$ W m^{-2}
Planetary emissivity	ϵ_P	0.55–0.60 *
Oceanic emissivity	ϵ_O	0.96
Atmospheric emissivity	ϵ_A	0.84
Planetary albedo	α_P	$0.7995 - 0.3615 \sin^2(\text{lat})$
Atmospheric absorptivity	$(1 - a)$	0.35 over ocean 1.0 over land
Atmospheric heat diffusivity	K_T	$0.5\text{–}10 \times 10^6$ m^2 s^{-1} *
Atmospheric moisture diffusivity	K_q	$0.5\text{–}10 \times 10^6$ m^2 s^{-1} *
Atmospheric scale height (temperature)	H_a	8.4 km
Atmospheric scale height (moisture)	H_q	1.8 km
Latent heat transfer coefficient	E_0	$1\text{–}50 \times 10^{-3}$ kg m^{-1} s^{-1} *
Sensible heat transfer coefficient	Q_0	10 Wm^{-2} K^{-1}
Atmospheric time step	Δt_A	6 hours

*Calculated at coupling with the oceanic steady state.

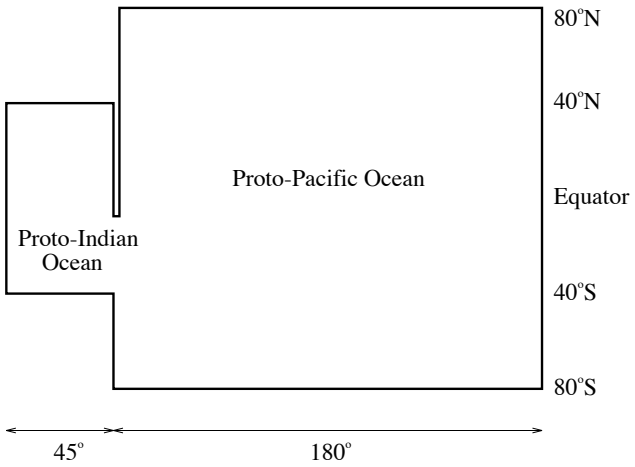

Figure 1. The ocean model domain used consists of two connected basins representing the "proto-Pacific" ocean which stretches from 80°S to 80°N with a width of 180°, and the "proto-Indian" ocean (45° width), which stretches from 40°S to 40°N. The two basins are linked by a strait extending from 40°S to 7.5°S, and the waters at these latitudes are assumed to be well mixed horizontally.

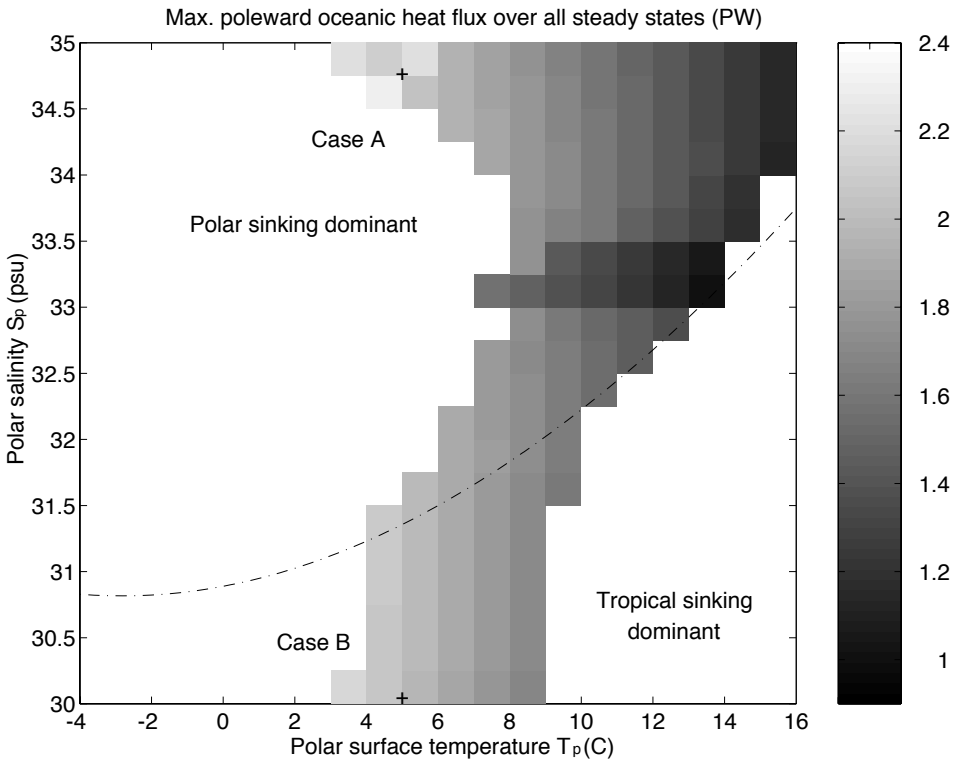

Figure 2. The shaded area represents the region of (T_p, S_p) space over which a consistent diffusive atmosphere can be found for the initial oceanic steady state. The equatorial temperature and salinity are fixed at 28°C and 36.5 psu respectively. The degree of shading indicates the maximum poleward oceanic heat transport for a given (T_p, S_p) pair over all the steady states found. The dot-dashed line divides roughly those states whose densest waters are at the tropics (below the line) from those whose densest waters are at the pole (above line). Finally, the two crosses marked case A and case B indicate the location in parameter space of the two examples illustrated later in the text.

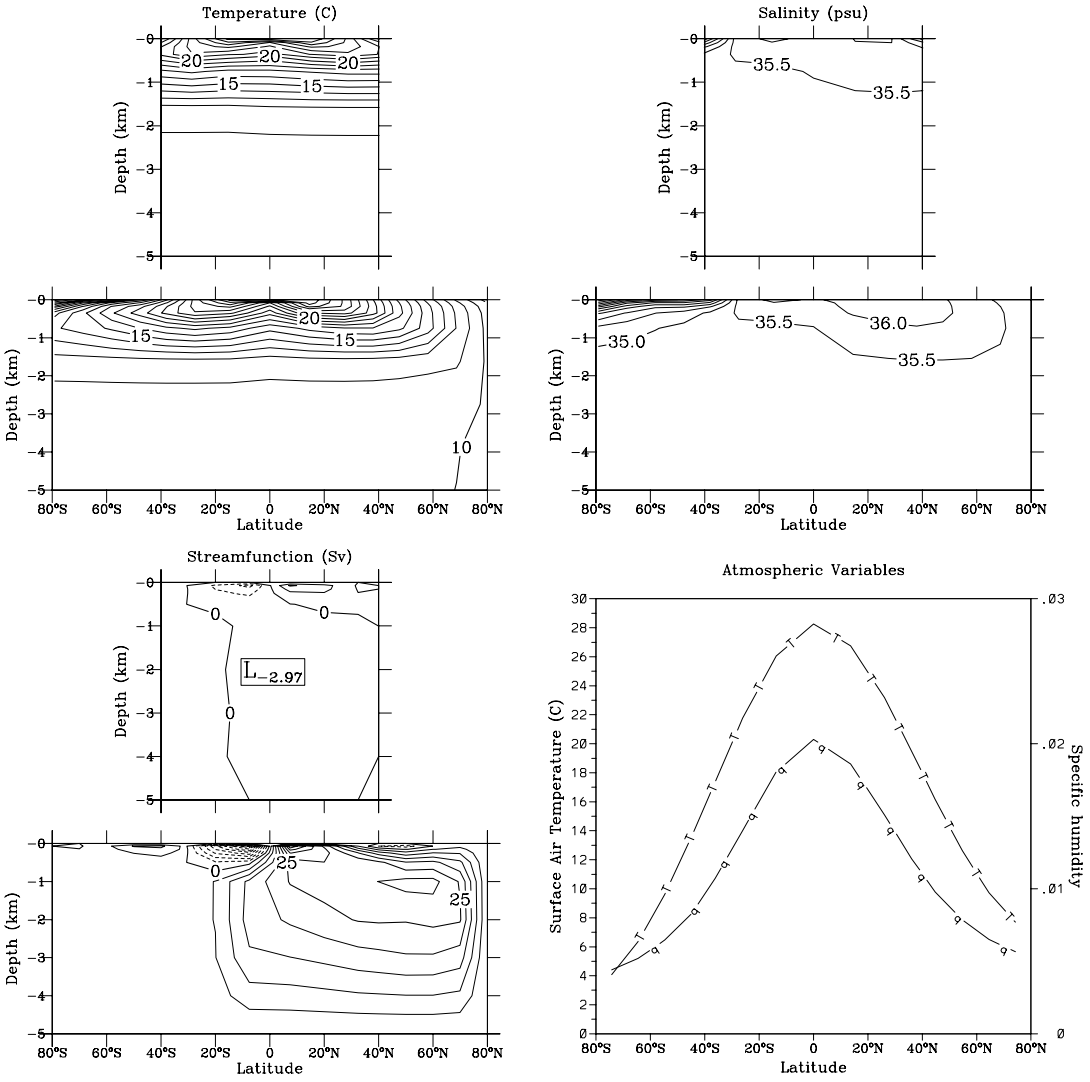

Figure 3. The two stable steady states for case A (T_p, S_p) =(5°C, 34.75 psu) looking westward through N-S sections of the Indian and Pacific oceans. The first state, (a) is characterised by deep sinking in the northern polar region, and the second, (b) by deep sinking at the southern mid-latitudes. There is a slight asymmetry (for both states) in the surface air temperature field because of the greater northward (first state) or southward (second state) oceanic heat transport. Bottom temperatures are around 10°C for (a) and 15°C for (b)

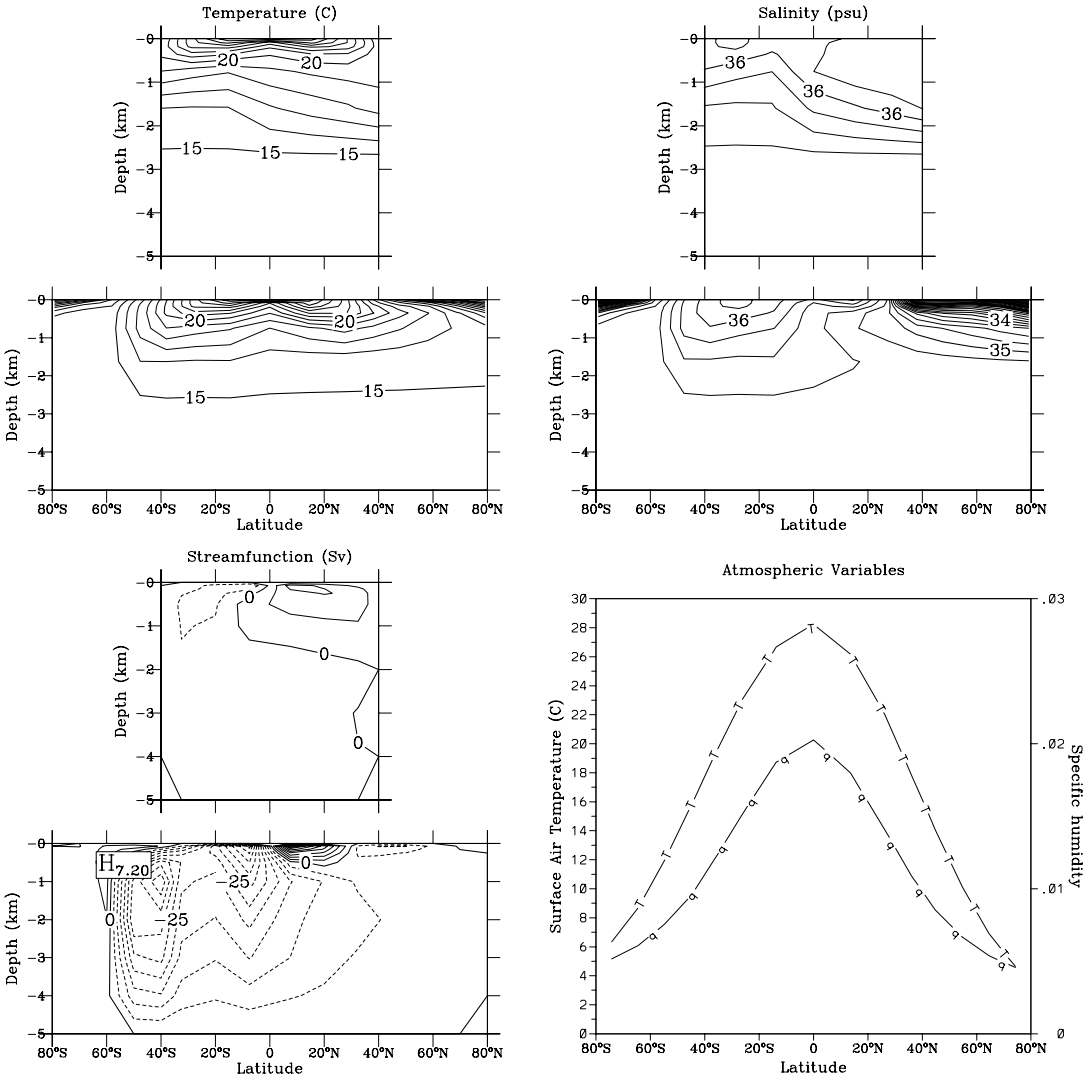
Temperature (C)
Salinity (psu)
Streamfunction (Sv)
Atmospheric Variables
Depth (km)
Latitude
Surface Air Temperature (C)
Specific humidity
80°S 60°S 40°S 20°S 0 20°N 40°N 60°N 80°N

Figure 3b:

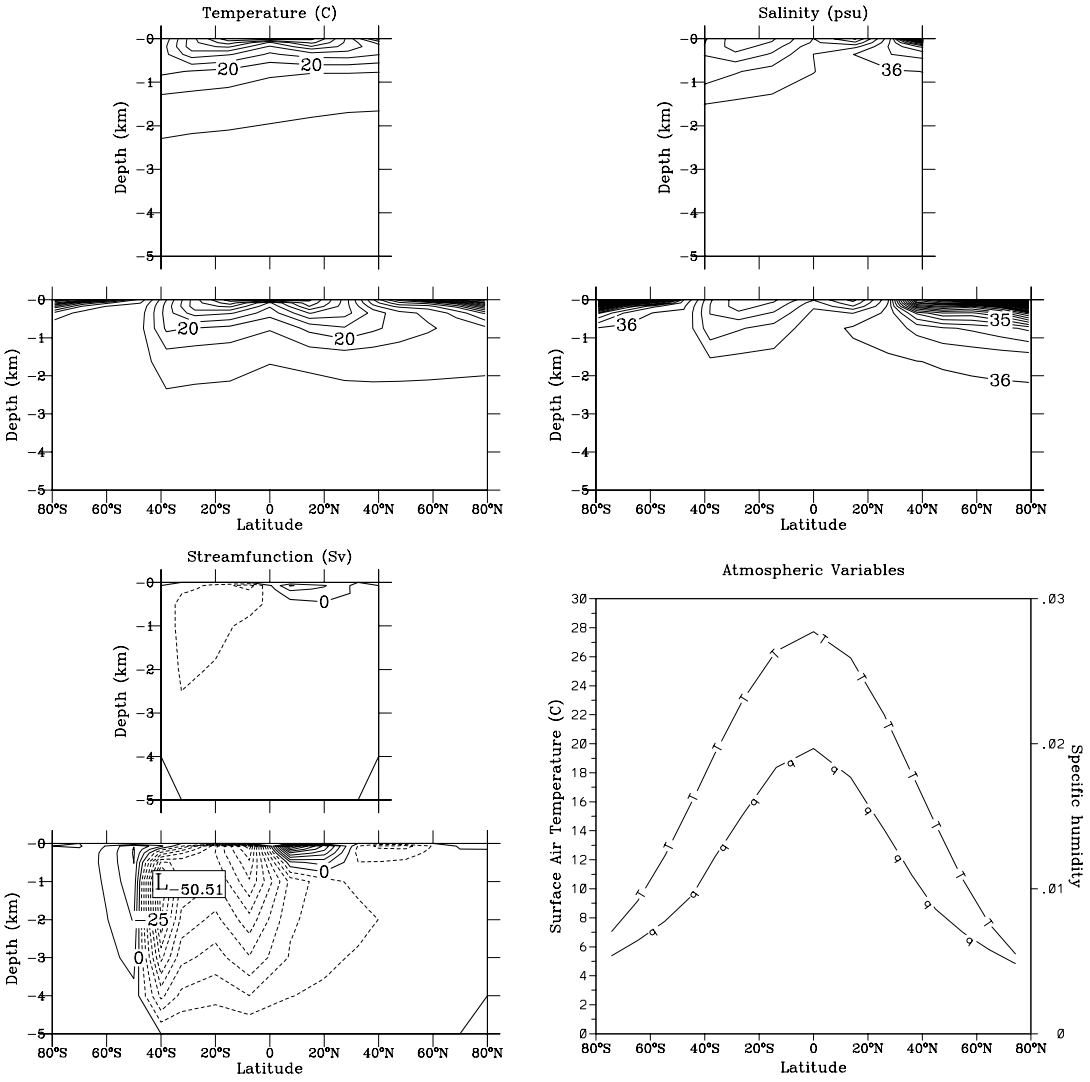

Figure 4. The stable steady states for case B (T_p, S_p) =(5°C, 30 psu). These states are characterised by sinking only at the (a) southern or (b) northern tropics. Again there is a slight asymmetry in the surface air temperature. The bottom waters are warm, just under 18°C.

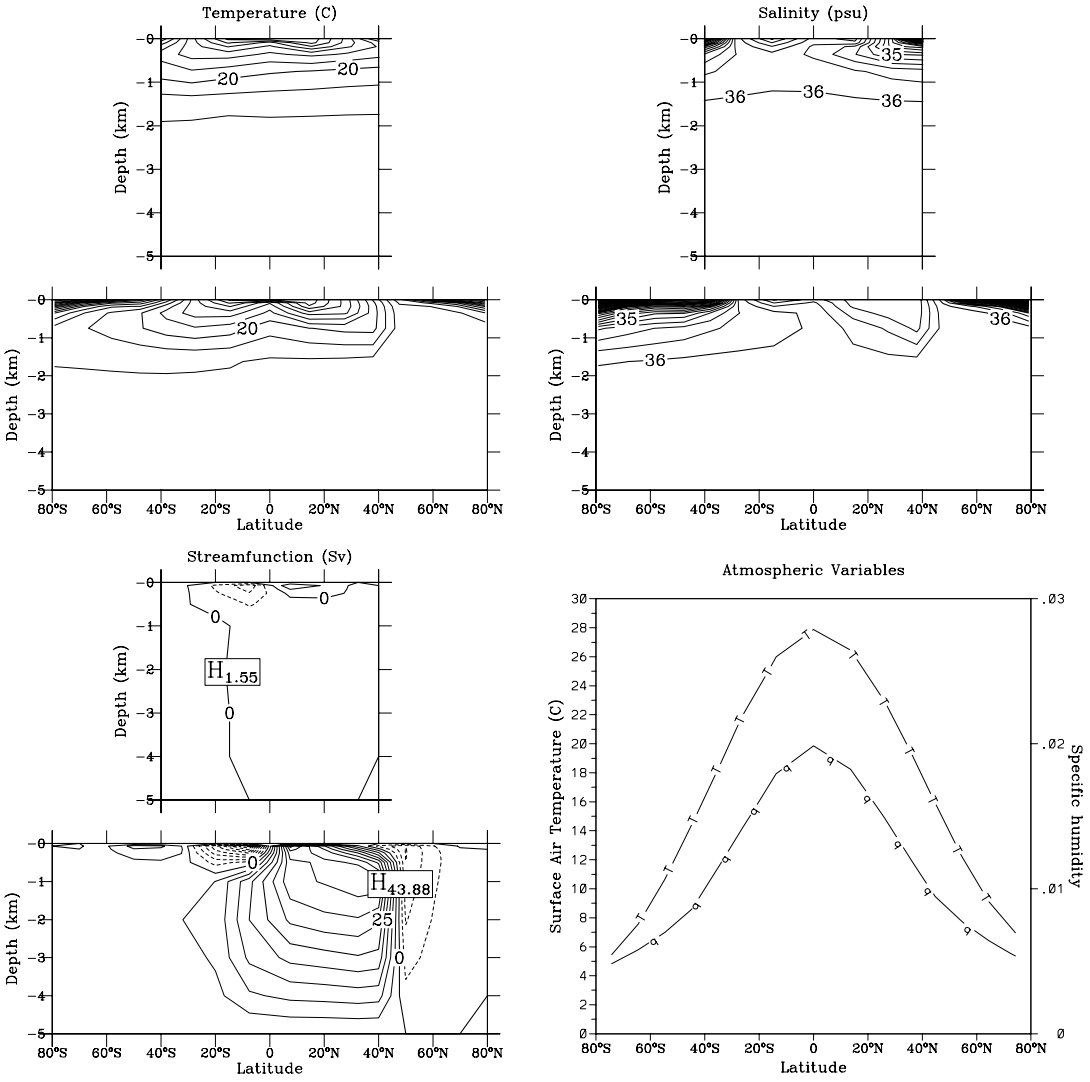
Temperature (C)
Salinity (psu)
Streamfunction (Sv)
Atmospheric Variables
Depth (km)
Latitude
Surface Air Temperature (C)
Specific humidity
H1.55
H43.88
80°S 60°S 40°S 20°S 0 20°N 40°N 60°N 80°N

Figure 4b:

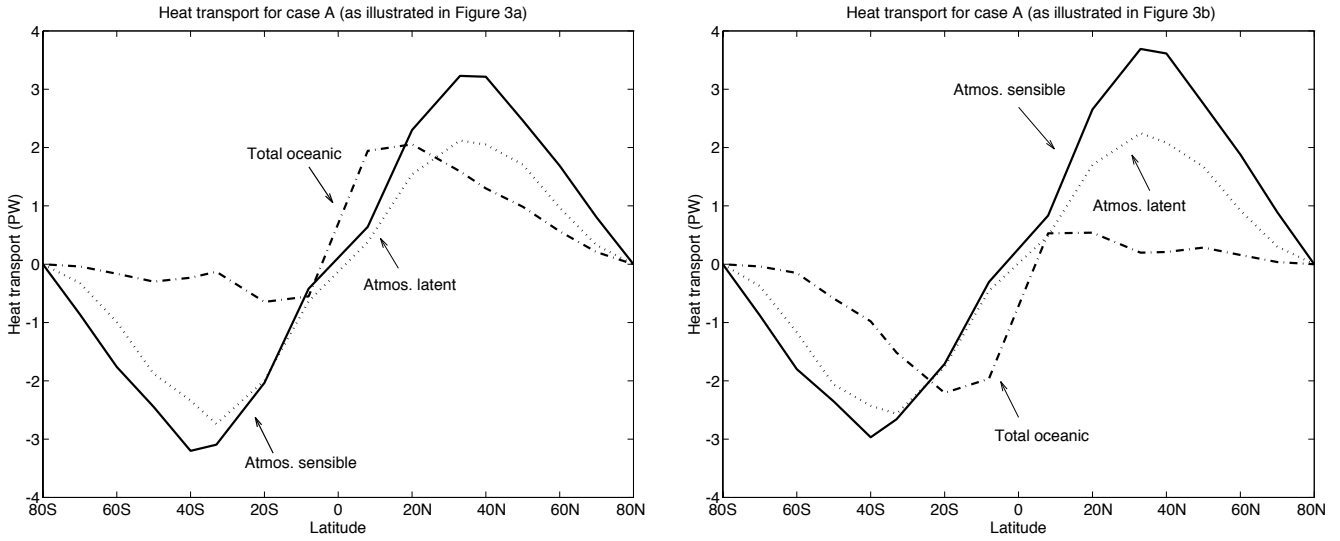

Figure 5. The zonal transport of heat by the oceans and by the atmosphere (broken down into sensible and latent heat components) for the stable steady states for case A illustrated in figs. 3a and b.

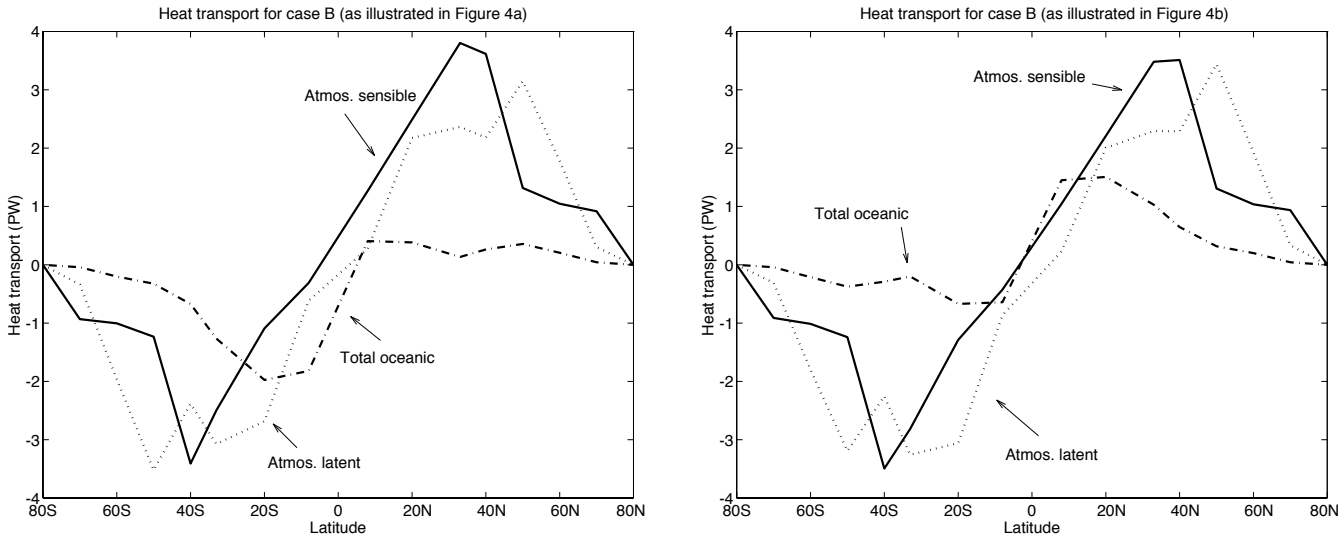

Figure 6. The zonal transport of heat by the oceans and by the atmosphere (broken down into sensible and latent heat components) for the stable steady states for case B illustrated in figs. 4a and b.